Nonlinear diffusion of negatively charged excitons in monolayer WSe_2

D. Beret,[1] L. Ren,[1] C. Robert,[1] L. Foussat,[1] P. Renucci,[1] D. Lagarde,[1] A. Balocchi,[1] T. Amand,[1] B. Urbaszek,[1] K. Watanabe,[2,3] T. Taniguchi,[2,3] X. Marie,[1] and L. Lombez[1]

[1]*Université de Toulouse, INSA-CNRS-UPS, LPCNO, 135 Av. Rangueil, 31077 Toulouse, France*

[2]*International Center for Materials Nanoarchitectonics, National Institute for Materials Science, 1-1 Namiki, Tsukuba 305-00044, Japan*

[3]*Research Center for Functional Materials, National Institute for Materials Science, 1-1 Namiki, Tsukuba 305-00044, Japan*

(Received 2 August 2022; revised 9 December 2022; accepted 22 December 2022; published 20 January 2023)

We investigate the diffusion process of negatively charged excitons (trions) in a WSe_2 transition-metal dichalcogenide monolayer. We measure the time-resolved photoluminescence spatial profiles of these excitonic complexes. They exhibit nonlinear diffusion corresponding to an effective negative diffusion behavior. Specifically, we examine the dynamics of the two negatively charged bright excitons (intervalley and intravalley trions) and of the dark trion. The time evolution allows us to identify the interplay of the different excitonic species: the trionic species appear after the neutral excitonic one. This is consistent with a bimolecular formation mechanism. Based on our experimental observations, we propose a phenomenological model suggesting the coexistence of two populations: a first one exhibiting a fast and efficient diffusion mechanism and a second one with a slower dynamics and a less efficient diffusion process. These two contributions could be, respectively, attributed to hot and cold trion populations.

DOI: 10.1103/PhysRevB.107.045420

I. INTRODUCTION

The great recent interest in transition-metal dichalcogenides (TMD) monolayers relies on their direct band gaps and a strong light-matter interaction, making these materials suitable for ultrathin optoelectronic devices [1]. The unusual optical and electrical properties of such monolayer semiconductors are related to the strong Coulomb interaction between electrons and holes in these materials, which opens new ways for the development of devices based on excitonic species rather than free carriers, even at room temperature. The investigation of the excitonic transport and unassisted diffusion is therefore an important topic. Only a few experimental works have achieved the control of the excitonic transport by applying electrical gates [2] or by modifying the local strain [3,4]. More studies have instead focused on the unassisted diffusion of several excitonic species [3–7]. Time- and spatially resolved diffusion experiments allow, in addition, the independent determination of the diffusion and recombination mechanisms (i.e., lifetimes) offering a deeper insight into the species transport mechanisms beyond a simple measurement of the diffusion length.

Although efficient excitonic transport has been reported, it turns out that the rich family of excitonic species can make the transport mechanism rather complex. Nonlinear diffusion processes have also been observed, essentially linked to the interactions between the different excitonic complexes [8–14]. For instance, the presence of nonequilibrium excitons can create a surprising halolike carrier profile induced by a hot population [8,11,15,16]. Such behavior might also be influenced by the dielectric environment as the monolayer encapsulation impacts on the transport mechanisms [17,18].

Another interesting phenomenon is effective negative diffusion in TMDs which leads to the narrowing of the spatial exciton distribution during diffusion, and finds its origins in the interplay of the excitonic species [19]. Effective negative diffusion has been experimentally observed in several semiconducting materials such as perovskites [19], TMDs [20], or organic semiconductor [21] at room temperature.

Here, we study a WSe_2 monolayer which offers a rich variety of excitonic complexes. We use a state-of-the-art charge-adjustable device and focus on the *n*-doped regime to probe the influence of electron doping on the excitonic transport properties. We investigate negatively charged excitons (trions) and bright and dark complexes at low temperature in photoluminescence experiments. Our study reveals a nonlinear transport behavior where an effective negative diffusion is observed. A simple diffusion model shows the coexistence of two populations which could be related to hot and cold trion populations. Their interplay with neutral excitons through bimolecular formation with resident electrons is also evidenced.

II. EXPERIMENTAL DETAILS

We study the charge-adjustable WSe_2 device sketched in Fig. 1(a). Details of the sample fabrication can be found elsewhere [22]. An electric bias can be applied to tune the carrier concentration. We focus our analysis on the *n*-doped regime [22–24]. Typical photoluminescence (PL) spectra as a function of the electron doping concentration are displayed in Fig. 1(c). Measurements are performed at $T = 4$ K with 5-μW excitation power provided by a He:Ne laser at $E_{ex} = 1.96$ eV. Several excitonic species are identified such as the bright neutral exciton X^0, the dark neutral exciton X^D, the bright negative trions (intervalley triplet X^{T-} and intravalley singlet X^{S-}, [see Fig. 1(b)] and the negatively charged dark trion X^{D-}

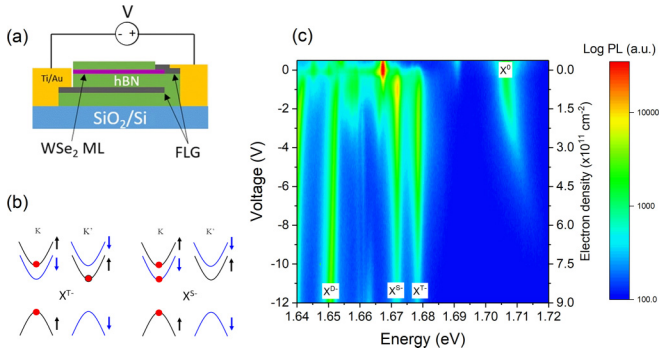

FIG. 1. (a) Scheme of the sample structure: ML = monolayer, FLG = few−layer graphene. (b) Sketch of the two negative trion configurations: triplet X^{T-} and singlet X^{S-}. (c) Color map showing the evolution of the PL spectra with the applied bias (resulting in an electrostatic doping).

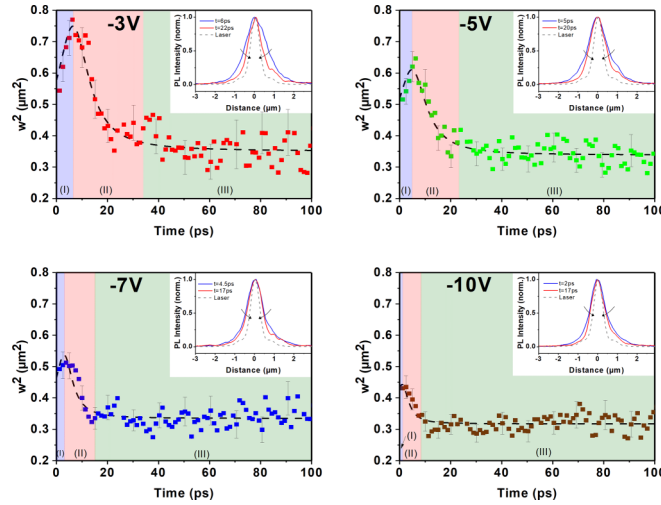

FIG. 2. Squared width of the PL spatial profile w^2 for the X^{T-} trion as a function of time. Temporal evolution is displayed for different biases from −3 to −10 V. Insets represent the spatial profiles at short times when w^2 is maximum and a few picoseconds later after the effective negative diffusion. The laser profile is displayed as a reference. Temporal regimes I (purple), II (red), and III (green) are indicated in each panel.

in agreement with previous reports [23,25–30]. The encapsulation in hexagonal boron nitride layers offers state-of-the art quality, as can be seen by the narrow optical transition linewidth of 2.5 meV for the neutral exciton X^0 transition [31].

In the following we mainly focus on the transport properties of the two bright trions (negatively charged exciton) X^{T-} and X^{S-}. As sketched in Fig. 1(b) the triplet X^{T-} is composed of a bright exciton and an electron in the opposite valley. In contrast, the singlet X^{S-} is composed of a bright exciton and a resident electron in the same valley. The photoluminescence experiment is based on a diffraction-limited laser excitation that induces lateral diffusion of the photogenerated species [32]. The excitonic complex of interest is spectrally selected by adding angle-tunable long- and short-pass interferential filters which transmit a spectral region as narrow as 6 meV (2.5 nm). We then used a Streak camera system to record the time evolution of the PL spatial profile [13]. The instrument response function has a full width at half maximum (FHWM) of 5.5 ps (see Fig. 3). The Ti: Sa laser excitation is set to $E_{el} = 1.79$ eV, with 80 MHz repetition frequency, 1.5 ps pulse width, and $\sim 1\mu J/cm^2$ pulse energy density. We have used a microscope objective with numerical aperture NA = 0.8. An ~ 700 nm FWHM excitation spot is measured from the laser intensity profile (insets of Fig. 2).

The spatiotemporal information allows separating the transport and the recombination mechanisms [33]. The PL spatial profile is considered as Gaussian, $\forall t \ : \ I_{PL}(x) \sim \exp(-\frac{x^2}{w^2})$, and we examine the squared width w^2 of the PL profile as a function of time $w^2(t)$ [33]. In case of linear broadening (i.e., classical diffusion process) an effective diffusion coefficient D can be extracted according to the relation $w^2(t) = 4Dt$ [33]. However, this simple relation is not applicable if nonlinear diffusion is observed.

We first describe in Fig. 2 the time dependence of w^2 for the X^{T-} trion for different electron doping densities. Note that similar observations are made for the X^{S-} trion with only a small difference on the dynamics due to their slightly different lifetimes (see Supplemental Material) [34]. Three regimes can be identified: (I) Within a few picoseconds we observe a fast broadening, which would indicate an efficient diffusion process with an effective diffusion coefficient close to 1000 cm²/s. For higher electron doping densities, this first regime becomes less and less visible, indicating a very fast diffusion. The PL profile becomes broader than the laser spot on a timescale shorter than our temporal resolution at the highest doping density. In the following 20 ps, a second regime (II) is visible with a clear reduction of the PL profile width, mimicking an effective negative diffusion process. The insets in Fig. 2 report the measured spatial profiles of w^2 at its maximum and a few picoseconds later to better illustrate this second regime. (III) Finally, on a longer timescale, we observe a weak diffusion process with a weak dependence on the electron doping.

We now describe the time-resolved photoluminescence data and we focus on the interplay of the excitonic species. Figure 3(a) shows the spatially integrated time evolution of the PL intensity (TRPL) for different biases for the excitonic complex X^{T-}, while Fig. 3(b) reports the TRPL intensity dependences for X^{D-}. The TRPL dynamics of the dark complexes are longer than the bright complexes' ones [22,23,35,36] and shows a rather monoexponential behavior. Another difference is the temporal evolution of the squared width w^2 for X^{D-} which show a linear dependence as shown in the inset of Fig. 3(b) for $V = 3$ V and in the Supplemental Material for all the voltages [34].

The X^{T-} TRPL exhibits a fast decay followed by a slow one; the fast dynamics becomes progressively shorter with increasing the electron concentration and mostly corresponds to the second regime (II) mentioned above (see Fig. 2). Zooming in on the first picoseconds [inset of Fig. 3(a)] we observe that negatively charged excitonic complexes appear with a clear delay after the emission of the neutral exciton. Note that all negatively charged excitonic complexes (X^{S-}, X^{T-}, X^{D-} not shown here) appear after the neutral exciton X^0. We also measure shorter delay times for higher doping. This observation is

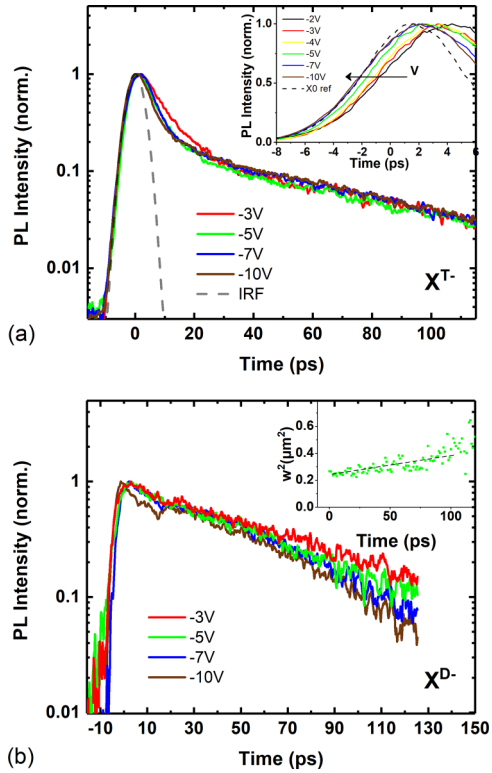

FIG. 3. (a) TRPL dynamics for X^{T-} at different biases. Inset : TRPL dynamics for the first picoseconds for X^{T-}. X^0 is shown as the time reference. (b) TRPL dynamics for X^{D-} at different biases. Inset: squared width w^2 of the PL profile as a function of time for $V = -3$ V.

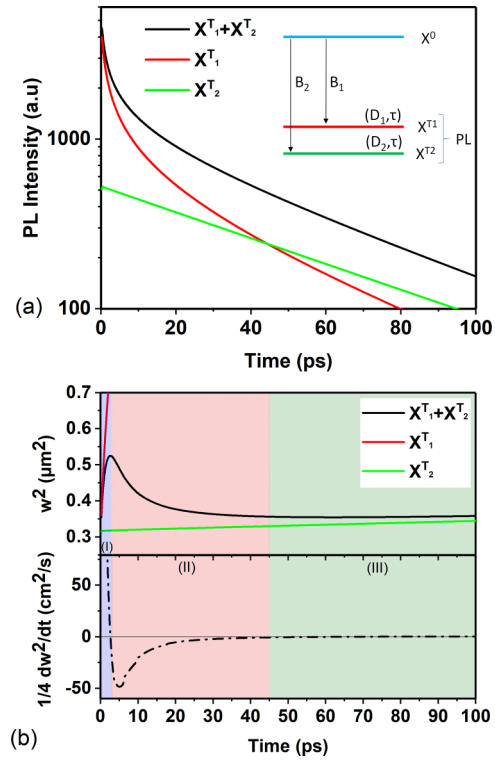

FIG. 4. (a) TRPL simulated signal for $I_{X^{T1}}$, $I_{X^{T2}}$, and $I_{PL} = I_{X^{T2}} + I_{X^{T1}}$ shown in semilogarithmic scale (b) Top: Simulated temporal evolution of the squared width w^2 of the PL spatial profiles; see text. Bottom: first derivative of the squared width w^2 to evidence the effective negative behavior of the diffusion process.

consistent with a bimolecular formation process of the trionic species between the neutral exciton and the resident electrons. A trimolecular formation process seems less probable as the TRPL signal of the trion in the early stage is negligible as compared to the X^0. Moreover, the laser excitation energy being below the band-gap energy [37], the geminate formation of the X^0 excitonic species is the most efficient mechanism [38], whereas the trimolecular formation of the trions from free charges is very unlikely under these excitation conditions.

III. DISCUSSION

We now discuss the origin of the nonlinear diffusion regime of the bright negatively charged excitons. We focus once again on the triplet X^{T-} but similar conclusions can be applied to the singlet X^{S-}. To model the effective negative diffusion the presence of one single population is insufficient. Indeed, the solution of the classical diffusion equation cannot result in effective negative diffusion, even considering a time-dependent diffusion coefficient. For instance, one can model a reduction of the diffusion coefficient when the carrier concentration is decreasing as it becomes more sensitive to potential fluctuations or defects [38]. But, even in this scenario, the temporal evolution of w^2 is slowed down but cannot decrease. A time-dependent diffusion coefficient modifies the PL profile broadening only in a monotonic way. A phenomenological explanation can be proposed admitting the contribution of two populations ($n_{X^{T1}}$ and $n_{X^{T2}}$), which cannot be spectrally distinguished within the ∼6-meV width of our spectral resolution, the first one having a *fast* diffusion mechanism combined with a shorter effective lifetime and a second one presenting a *slow* diffusion process and a longer effective lifetime. In this case, the first population contributes to the rapid increase of w^2 while vanishing quickly to make room for the second contribution having a weak role on the diffusion process.

In order to qualitatively model the nonlinear diffusion with an effective negative diffusion deriving from the existence of the two contributing populations $n_{X^{T1}}$ and $n_{X^{T2}}$ we develop the following rate-equation model:

$$\frac{dn_{X^0}}{dt} = G + \overrightarrow{\nabla}_r.[D_{X^0}\overrightarrow{\nabla}_r n_{X^0}] - \frac{n_{X^0}}{\tau_{X^0}} - B_1 n_{X^0} n_{e^-} - B_2 n_{X^0} n_{e^-},$$

$$\frac{dn_{X^{T1}}}{dt} = \overrightarrow{\nabla}_r[D_{X^{T1}}\overrightarrow{\nabla}_r n_{X^{T1}}] - \frac{n_{X^{T1}}}{\tau_{X^{T1}}} + B_1 n_{X^0} n_{e^-},$$

$$\frac{dn_{X^{T2}}}{dt} = \overrightarrow{\nabla}_r[D_{X^{T2}}\overrightarrow{\nabla}_r n_{X^{T2}}] - \frac{n_{X^{T2}}}{\tau_{X^{T2}}} + B_2 n_{X^0} n_{e^-},$$

where G is the generation rate of neutral excitons. $n_{X^{T1}}$ and $n_{X^{T2}}$ populations are determined from the neutral exciton density n_{X^0} via a bimolecular formation with the electron reservoir n_{e-} [see scheme in Fig. 4(a)]. The two populations arise from the solution of the simple diffusion equation in polar coordinates when considering similar global recombination lifetimes $\tau_{X^{T1}} = \tau_{X^{T2}}$ but different diffusion coefficients

$D_{X^{T1}} \neq D_{X^{T2}}$. Note that although $\tau_{X^{T1}} = \tau_{X^{T2}}$ the effective lifetime of the two populations is different [see Fig. 4(a)] since the temporal dependence is linked to the spatial dependence.

Solving these equations yields a space-time evolution of the trion PL intensity $I_{\mathrm{PL}}(r,t) \propto n_{X^{T1}} + n_{X^{T2}}$. We then extract the temporal dependence of the spatial PL profile with the same method used to treat the experimental data. The modeling of $w^2(t)$ for each individual trion contribution as well as for their sum (i.e., the PL intensity) is presented in Fig. 4(b). A satisfactory qualitative agreement is found with our experimental data. The lifetime values are extracted from our TRPL data, whose values are consistent with those found in the literature, i.e., $\tau_{X^0} = 1$ ps and $\tau_{X^{T1}} = \tau_{X^{T2}} = 60$ ps [22]. The bimolecular recombination coefficients are $B_1 = 0.9 \times 10^{-11}\,\mathrm{cm}^2/\mathrm{ps}$ and $B_2 = 0.1 \times 10^{-11}\,\mathrm{cm}^2/\mathrm{ps}$ [22]. The extracted diffusion coefficients $D_{X^0} = D_{X^{T2}} = 1\,\mathrm{cm}^2/\mathrm{s}$ are typical for excitonic species [17], while $D_{X^{T1}} = 1000\,\mathrm{cm}^2/\mathrm{s}$ is much larger. However, this high value can also be evaluated by considering a linear diffusion process in the first picoseconds (region I) from the relation $w^2 = 4Dt$. Such high values have already been reported for instance for the room-temperature diffusion of hot excitons in WS_2 [20].

To better illustrate the role of the two populations in the nonlinear diffusion process, we plot in Fig. 4(a) the simulated TRPL signals I_{PL} for $V = -3$ V as well as the contribution of the populations $I_{\mathrm{PL}} = I_{X^{T2}} + I_{X^{T1}}$. Figure 4(b) reproduces the temporal evolution of w^2. The colored shaded areas represent the time boundaries of the three regimes experimentally observed. Consistent with the experimental results, the first regime (region I) shows a positive and rapid classical diffusion. This is then followed by an effective negative diffusion behavior (region II). The change between the two regimes occurs when the contribution of the X^{T1} *PL* intensity becomes small enough to observe the PL intensity due to X^{T2}. Finally, a small variation of w^2 is observed after a certain delay (region III) where the contribution of X^{T1} becomes negligible compared to X^{T2}. Note that if we could experimentally distinguish the individual contributions of the two populations, we would obtain the two populations' w^2 dependences displayed in the top of Fig. 4(b) : red for the X^{T1} PL signal and green for the X^{T2} one. The fast contribution would result in an effective diffusion coefficient $D_{\mathrm{fast}} \sim 450\,\mathrm{cm}^2/\mathrm{s}$ using the linear relation $w^2 = 4Dt$, while an effective diffusion coefficient $D_{\mathrm{slow}} \sim 3\,\mathrm{cm}^2/\mathrm{s}$ is obtained considering the slow contribution of X^{T2}. The bottom of Fig. 4(b) represents the first derivative of the total $w^2 = w^2_{\mathrm{fast}} + w^2_{\mathrm{slow}}$ to better appreciate the change from a positive to a negative effective diffusion behavior.

Although the three-population model reproduces the experimental nonlinear behavior with a relatively good agreement, the influence of the electron doping cannot be reproduced. This model is quite insensitive to the variation of n_{e-}. Indeed, a change of the latter parameter has a weak influence on the ratio $n_{X^{T1}}(t)/n_{X^{T2}}(t)$ which is responsible for the change of $w^2(t)$ (see Supplemental Material (SM) for details [34]). In order to improve the model, we introduce two neutral excitonic populations: a hot and a cold exciton population, as already considered for the interpretation of diffusion process in a previous study [38]. In this case, splitting the first equation of the population n_{X^0} in two parts (see SM), allows for the

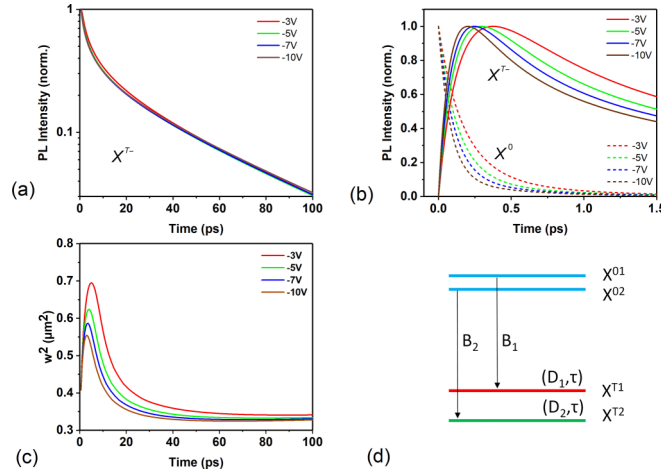

FIG. 5. (a) TRPL simulated signal for X^{T-} for different biases (resulting in different electron doping densities). (b) TRPL simulated signals in the first picoseconds for X^0 and for X^{T-} at different biases. (c) Simulated temporal evolution of the PL profile with w^2 for different biases. (d) Sketch of the energy levels used in the model showing the two trion populations X^{T1} and X^{T2} as well as the two neutral exciton populations X^{01} and X^{02}.

reproduction of the voltage dependence as seen in Fig. 5. The results shown have been obtained setting $D_{X^{T1}} = D_{X^{01}}$ and $D_{X^{T2}} = D_{X^{02}}$.

As the electron doping is increased, the contribution of X^{T2} population (with small $D_{X^{T2}}$) becomes dominant at shorter times (with respect to X^{T1} population) which weakens and shortens the first regime of efficient diffusion [see Fig. 5(c)] as $D_{X^{T2}} < D_{X^{T1}}$. It is evidenced by the voltage dependence of the ratio $n_{X^{T1}}(t)/n_{X^{T2}}(t)$; see SM for details [34].

TRPL data are also reproduced with a good agreement as observed in Fig. 5(a), where a slight variation of the dynamics with the bias is seen at short time. In particular, the time delay between the neutral exciton X^0 PL emission and the trion PL emission is also found to be reduced as the electron doping concentration is increased [see Fig. 5(b)]. These results are in agreement with the experimental observations [inset of Fig. 3(a)].

The origin of the two trions' populations is still unclear. As mentioned earlier, it is unlikely that the experimental results are related to defects or disorder as a unique diffusion coefficient cannot reproduce the experimental observation. This is also consistent with the narrow PL linewidths of the excitonic species which suggest a high-quality sample. One possibility would be the presence of hot- and cold trion populations that cannot be distinguished within the 6-meV width of our spectral window. A hot population of trionic species has been shown to slightly increase the PL spectral width at low energy [39] and its dynamics can correspond to what has been theoretically reported for WSe_2 [40], especially this material having a hot population lifetime of a few picoseconds. This hypothesis is also supported by the experimental observation of excitonic complexes at 300 K in perovskite materials [19] and WS_2 [20]. Moreover, some theorical investigations on the effective negative diffusion for excitons also put forward thermalization mechanisms with intervalley exciton-phonon scattering [41] or interaction with the electron gas [42]; also

see Supplemental Material [34]. Finally, we point out that no effective negative diffusion is seen on the negatively charged dark trion species. This might be explained by its relatively long lifetime where efficient thermalization might occur before recombination. The monoexponential TRPL signal of this excitonic complex could also be an indication of the relaxation of a single population as compared to the negatively charged bright excitons for which a roughly biexponential decay is observed. The diffusion coefficient of X^{D-} is slightly reduced by the electron doping (see Supplemental Material [34]), which would be consistent with a reduction of the thermalization while increasing the cold electronic reservoir. Overall, the experimental data and the model suggest the existence of efficient transport mechanisms assisted by hot population. These effects are only visible if the effective lifetime of the excitonic complex is sufficiently small compared to the thermalization time. To confirm this hypothesis, a pump-probe experiment combining picosecond time resolution and a meV spectral resolution could be performed in the future.

IV. CONCLUSION

We have investigated the transport properties of negatively charged excitonic complexes in WSe_2 monolayers. A nonlinear diffusion process is revealed for the two bright trions where an effective negative diffusion is evidenced. A phenomenological model highlights the contribution of two populations with, respectively, a fast and efficient diffusion mechanism for the first one and a slow but inefficient diffusion mechanism for the second one. The coexistence of two populations might also be present for the neutral exciton and could originate from a hot and cold populations. As a general trend, hot populations would have a large diffusion coefficient before they thermalize. Although this hypothesis might require further experimental studies, our results indicate that an efficient transport mechanism in TMD materials can be tuned by controlling the thermalization rate.

ACKNOWLEDGMENTS

This study has been partially supported through the EUR NanoX Grant No. ANR-17-EURE-0009 in the framework of the "Programme des Investissements d'Avenir." We thank F. Cadiz for fruitful discussions. This work was also supported by Agence Nationale de la Recherche funding ANR SIZMO2D, ANR ICEMAN, ANR ATOEMS, and ANR IXTASE.

[1] G. Wang, A. Chernikov, M. M. Glazov, T. F. Heinz, X. Marie, T. Amand, and B. Urbaszek, Colloquium: Excitons in atomically thin transition metal dichalcogenides, Rev. Mod. Phys. **90**, 021001 (2018).

[2] D. Unuchek, A. Ciarrocchi, A. Avsar, K. Watanabe, T. Taniguchi, and A. Kis, Room-temperature electrical control of exciton flux in a van der Waals heterostructure, Nature (London) **560**, 340 (2018).

[3] F. Cadiz, C. Robert, E. Courtade, M. Manca, L. Martinelli, T. Taniguchi, K. Watanabe, T. Amand, A. C. H. Rowe, D. Paget *et al.*, Exciton diffusion in WSe_2 monolayers embedded in a van der Waals heterostructure, Appl. Phys. Lett. **112**, 152106 (2018).

[4] N. Kumar, Q. Cui, F. Ceballos, D. He, Y. Wang, and H. Zhao, Exciton diffusion in monolayer and bulk $MoSe_2$, Nanoscale **6**, 4915 (2014).

[5] T. Kato and T. Kaneko, Transport Dynamics of Neutral Excitons and Trions in Monolayer WS_2, ACS Nano **10**, 9687 (2016).

[6] L. Yuan, T. Wang, T. Zhu, M. Zhou, and L. Huang, Exciton dynamics, transport, and annihilation in atomically thin two-dimensional semiconductors, J. Phys. Chem. Lett. **8**, 3371 (2017).

[7] J. He, D. He, Y. Wang, Q. Cui, F. Ceballos, and H. Zhao, Spatiotemporal dynamics of excitons in monolayer and bulk WS_2, Nanoscale **7**, 9526 (2015).

[8] R. Rosati, K. Wagner, S. Brem, R. Perea-Causín, J. D. Ziegler, J. Zipfel, T. Taniguchi, K. Watanabe, A. Chernikov, and E. Malic, Non-equilibrium diffusion of dark excitons in atomically thin semiconductors, Nanoscale **13**, 19966 (2021).

[9] K. Wagner, J. Zipfel, R. Rosati, E. Wietek, J. D. Ziegler, S. Brem, R. Perea-Causín, T. Taniguchi, K. Watanabe, M. M. Glazov *et al.*, Nonclassical Exciton Diffusion in Monolayer WSe_2, Phys. Rev. Lett. **127**, 076801 (2021).

[10] M. M. Glazov, Quantum Interference Effect on Exciton Transport in Monolayer Semiconductors, Phys. Rev. Lett. **124**, 166802 (2020).

[11] R. Perea-Causín, S. Brem, R. Rosati, R. Jago, M. Kulig, J. D. Ziegler, J. Zipfel, A. Chernikov, and E. Malic, Exciton propagation and halo formation in two-dimensional materials, Nano Lett. **19**, 7317 (2019).

[12] J. Wang, Y. Guo, Y. Huang, H. Luo, X. Zhou, C. Gu, and B. Liu, Diffusion dynamics of valley excitons by transient grating spectroscopy in monolayer WSe_2, Appl. Phys. Lett. **115**, 131902 (2019).

[13] M. Kulig, J. Zipfel, P. Nagler, S. Blanter, C. Schüller, T. Korn, N. Paradiso, M. M. Glazov, and A. Chernikov, Exciton Diffusion and Halo Effects in Monolayer Semiconductors, Phys. Rev. Lett. **120**, 207401 (2018).

[14] S. Mouri, Y. Miyauchi, M. Toh, W. Zhao, G. Eda, and K. Matsuda, Nonlinear photoluminescence in atomically thin layered WSe_2 arising from diffusion-assisted exciton-exciton annihilation, Phys. Rev. B **90**, 155449 (2014).

[15] M. M. Glazov, Phonon wind and drag of excitons in monolayer semiconductors, Phys. Rev. B **100**, 045426 (2019).

[16] D. F. Cordovilla Leon, Z. Li, S. W. Jang, and P. B. Deotare, Hot exciton transport in WSe_2 monolayers, Phys. Rev. B **100**, 241401(R) (2019).

[17] J. Zipfel, M. Kulig, R. Perea-Causín, S. Brem, J. D. Ziegler, R. Rosati, T. Taniguchi, K. Watanabe, M. M. Glazov, E. Malic, and A. Chernikov, Exciton diffusion in monolayer semiconductors with suppressed disorder, Phys. Rev. B **101**, 115430 (2020).

[18] C. R. Dean, A. F. Young, I. Meric, C. Lee, L. Wang, S. Sorgenfrei, K. Watanabe, T. Taniguchi, P. Kim, K. L. Shepard *et al.*, Boron nitride substrates for high-quality graphene electronics, Nat. Nanotechnol. **5**, 722 (2010).

[19] J. D. Ziegler, J. Zipfel, B. Meisinger, M. Menahem, X. Zhu, T. Taniguchi, K. Watanabe, O. Yaffe, D. A. Egger,

and A. Chernikov, Fast and anomalous exciton diffusion in two-dimensional hybrid perovskites, Nano Lett. **20**, 6674 (2020).

[20] Q. Liu, K. Wei, Y. Tang, Z. Xu, X. Cheng, and T. Jiang, Visualizing hot-carrier expansion and cascaded transport in WS_2 by ultrafast transient absorption microscopy, Adv. Sci. **9**, 2105746 (2022).

[21] A. M. Berghuis, T. V. Raziman, A. Halpin, S. Wang, A. G. Curto, and J. G. Rivas, Effective negative diffusion of singlet excitons in organic semiconductors, J. Phys. Chem. Lett. **12**, 1360 (2021).

[22] C. Robert, S. Park, F. Cadiz, L. Lombez, L. Ren, H. Tornatzky, A. Rowe, D. Paget, F. Sirotti, M. Yang *et al.*, Spin/valley pumping of resident electrons in WSe_2 and WS_2 monolayers, Nat. Commun. **12**, 5455 (2021).

[23] E. Liu, J. van Baren, Z. Lu, M. M. Altaiary, T. Taniguchi, K. Watanabe, D. Smirnov, and C. H. Lui, Gate Tunable Dark Trions in Monolayer WSe_2, Phys. Rev. Lett. **123**, 027401 (2019).

[24] Z. Li, T. Wang, Z. Lu, M. Khatoniar, Z. Lian, Y. Meng, M. Blei, T. Taniguchi, K. Watanabe, S. A. McGill *et al.*, Direct observation of gate-tunable dark trions in monolayer WSe_2, Nano Lett. **19**, 6886 (2019).

[25] A. M. Jones, H. Yu, J. R. Schaibley, J. Yan, D. G. Mandrus, T. Taniguchi, K. Watanabe, H. Dery, W. Yao, and X. Xu, Excitonic luminescence upconversion in a two-dimensional semiconductor, Nat. Phys. **12**, 323 (2016).

[26] E. Courtade, M. Semina, M. Manca, M. M. Glazov, C. Robert, F. Cadiz, G. Wang, T. Taniguchi, K. Watanabe, M. Pierre *et al.*, Charged excitons in monolayer WSe_2: Experiment and theory, Phys. Rev. B **96**, 085302 (2017).

[27] G. Wang, C. Robert, M. M. Glazov, F. Cadiz, E. Courtade, T. Amand, D. Lagarde, T. Taniguchi, K. Watanabe, B. Urbaszek *et al.*, In-Plane Propagation of Light in Transition Metal Dichalcogenide Monolayers: Optical Selection Rules, Phys. Rev. Lett. **119**, 047401 (2017).

[28] X.-X. Zhang, T. Cao, Z. Lu, Y.-C. Lin, F. Zhang, Y. Wang, Z. Li, J. C. Hone, J. A. Robinson, D. Smirnov *et al.*, Magnetic brightening and control of dark excitons in monolayer WSe_2, Nat. Nanotechnol. **12**, 883 (2017).

[29] Y. Zhou, G. Scuri, D. S. Wild, A. A. High, A. Dibos, L. A. Jauregui, C. Shu, K. De Greve, K. Pistunova, A. Y. Joe *et al.*, Probing dark excitons in atomically thin semiconductors via near-field coupling to surface plasmon polaritons, Nat. Nanotechnol. **12**, 856 (2017).

[30] M. He, P. Rivera, D. Van Tuan, N. P. Wilson, M. Yang, T. Taniguchi, K. Watanabe, J. Yan, D. G. Mandrus, H. Yu *et al.*, Valley phonons and exciton complexes in a monolayer semiconductor, Nat. Commun. **11**, 618 (2020).

[31] F. Cadiz, E. Courtade, C. Robert, G. Wang, Y. Shen, H. Cai, T. Taniguchi, K. Watanabe, H. Carrere, D. Lagarde *et al.*, Excitonic Linewidth Approaching the Homogeneous Limit in MoS2-Based van der Waals Heterostructures, Phys. Rev. X **7**, 021026 (2017).

[32] I. Favorskiy, D. Vu, E. Peytavit, S. Arscott, D. Paget, and A. C. H. Rowe, Circularly polarized luminescence microscopy for the imaging of charge and spin diffusion in semiconductors, Rev. Scienti. Inst. **81**, 103902 (2010).

[33] S. M. Sze and K. K. Ng, Physics and Properties of Semiconductors–A Review, *Physics of Semiconductor Devices*, 3rd ed. (John Wiley & Sons, Ltd, Hoboken, NJ, 2007), pp. 5–75.

[34] See Supplemental Material at http://link.aps.org/supplemental/10.1103/PhysRevB.107.045420 for a detailed comparison of the models, a discussion of the data vs the four-population model, and to see data from the negatively charged trion.

[35] J. Zipfel, K. Wagner, J. D. Ziegler, T. Taniguchi, K. Watanabe, M. A. Semina, and A. Chernikov, Light–matter coupling and non-equilibrium dynamics of exchange-split trions in monolayer WS_2, J. Chem. Phys. **153**, 034706 (2020).

[36] C. Robert, T. Amand, F. Cadiz, D. Lagarde, E. Courtade, M. Manca, T. Taniguchi, K. Watanabe, B. Urbaszek, and X. Marie, Fine structure and lifetime of dark excitons in transition metal dichalcogenide monolayers, Phys. Rev. B **96**, 155423 (2017).

[37] M. Goryca, J. Li, A. V. Stier, T. Taniguchi, K. Watanabe, E. Courtade, S. Shree, C. Robert, B. Urbaszek, X. Marie *et al.*, Revealing exciton masses and dielectric properties of monolayer semiconductors with high magnetic fields, Nat. Commun. **10**, 4172 (2019).

[38] H. P. Pasanen, M. Liu, H. Kahle, P. Vivo, and N. V. Tkachenko, Fast non-ambipolar diffusion of charge carriers and the impact of traps and hot carriers on it in CsMAFA perovskite and GaAs, Mater. Adv. **2**, 6613 (2021).

[39] A. Esser, E. Runge, R. Zimmermann, and W. Langbein, Photoluminescence and radiative lifetime of trions in GaAs quantum wells, Phys. Rev. B **62**, 8232 (2000).

[40] M. Yang, L. Ren, C. Robert, D. Van Tuan, L. Lombez, B. Urbaszek, X. Marie, and H. Dery, Relaxation and darkening of excitonic complexes in electrostatically doped monolayer WSe_2: Roles of exciton-electron and trion-electron interactions, Phys. Rev. B **105**, 085302 (2022).

[41] R. Rosati, R. Perea-Causín, S. Brem, and E. Malic, Negative effective excitonic diffusion in monolayer transition metal dichalcogenides, Nanoscale **12**, 356 (2020).

[42] R. A. Suris, V. P. Kochereshko, G. V. Astakhov, D. R. Yakovlev, W. Ossau, J. Nürnberger, W. Faschinger, G. Landwehr, T. Wojtowicz, G. Karczewski *et al.*, Excitons and trions modified by interaction with a two-dimensional electron gas, Phys. Status Solidi B **227**, 343 (2001).